Synthesis and Utilization of Monodisperse Superparamagnetic Colloidal Particles for Magnetically Controllable Photonic Crystals

Xiangling Xu,[†] Gary Friedman,[‡] Keith D. Humfeld,[§] Sara A. Majetich,[§] and Sanford A. Asher*,[†]

Department of Chemistry, University of Pittsburgh, Pittsburgh, Pennsylvania 15260, Electrical Engineering and Computer Science Department, University of Illinois, Chicago, Illinois 60607, and Department of Physics, Carnegie Mellon University, Pittsburgh, Pennsylvania 15213

Received August 27, 2001

We demonstrate fabrication of novel magnetically controllable photonic crystals formed through the self-assembly of highly charged, monodisperse superparamagnetic colloidal spheres. These superparamagnetic monodisperse charged polystyrene particles containing nanoscale iron oxide nanoparticles were synthesized through emulsion polymerization. They self-assemble into crystalline colloidal arrays (CCAs) in deionized water and Bragg diffract visible light. The diffraction from these superparamagnetic CCAs can be controlled by imposition of magnetic fields, which readily alter the CCA lattice constant. We also observe magnetically induced self-assembly of these superparamagnetic particles into CCAs in media such as NaCl aqueous solutions and organic polar solvents, which normally do not permit spontaneous CCA self-assembly. We also find that magnetic fields can strain the face-centered cubic lattice of superparamagnetic CCAs polymerized within hydrogels.The lattice symmetry of this photonic crystal becomes tetragonal. The observed magnetically induced CCA self-assembly enables the development of novel photonic crystal materials and devices.

Monodisperse highly charged colloidal particles spontaneously self-assemble into face-centered cubic (fcc) or body-centered cubic (bcc) crystalline colloidal arrays (CCAs) in low ionic strength aqueous solutions.[1−8] The optical dielectric constant of these colloidal particles, in general, differs from that of the surrounding medium, which results in a periodic variation in the material's refractive index. Similar to the diffraction of X-rays from atomic and molecular crystals, the resulting CCAs Bragg diffract UV, visible, or near-IR light, depending on their lattice constant. These CCAs are the simplest photonic crystals to show band gaps for propagation of electromagnetic radiation in particular directions.[4,6−13]

These CCA photonic crystal materials are of interest because they strongly interact with light and their diffracting periodic structure self-assembles. CCAs that are 100 μm thick show narrow diffraction bands (∼5 nm bandwidths) with transmittances[4] of less than 10^{-7}. We demonstrated earlier that these CCAs could be used as optical notch filters to filter out narrow wavelength intervals.[4,6,14,15] In addition, we have been developing these materials for nonlinear optical limiters and switches by making the refractive index of the colloidal particles nonlinear with respect to the incident light intensity.[16−18]

In addition to their utility for fabricating classical optical devices, there is also the possibility that these CCAs could be used to chemically fabricate 3-D photonic band gap materials.[19−24] These 3-D photonic band gap materials would have no eigenmodes for propagation of

* To whom correspondence should be addressed. Tel: (412) 624-8570. Fax: (412) 624−0588. E-mail: asher@pitt.edu.
[†] University of Pittsburgh.
[‡] University of Illinois.
[§] Carnegie Mellon University.

(1) Krieger, I. M.; O'Neill, F. M. *J. Am. Chem. Soc.* **1968**, *90*, 3114−3120.
(2) Hiltner, P. A.; Krieger, I. M. *J. Phys. Chem.* **1969**, *73*, 2386−2389.
(3) Carlson, R. J.; Asher, S. A. *Appl. Spectrosc.* **1984**, *38*, 297−304.
(4) Rundquist, P. A.; Photinos, P.; Jagannathan, S.; Asher, S. A. *J. Chem. Phys.* **1989**, *91*, 4932−4941.
(5) Spry, R. J.; Kosan, D. J. *Appl. Spectrosc.* **1986**, *40*, 782.
(6) Asher, S. A. U.S. Patents 4,627,689, 1986 and 4,632,517, 1986.
(7) Tarhan, I. I.; Watson, G. H. *Phys. Rev. Lett.* **1996**, *76*, 315−318.
(8) Pradhan, R. D.; Bloodgood, J. A.; Watson, G. H. *Phys. Rev. B* **1997**, *55*, 9503−9507.
(9) Biswas, R.; Sigalas, M. M.; Subramania, G.; Ho, K. M. *Phys. Rev. B* **1998**, *57*, 3701−3705.
(10) Busch, K.; John, S. *Phys. Rev. E* **1998**, *58*, 3896−3905.
(11) Rundquist, P. A.; Jagannathan, S.; Kasavamoorthy, R.; Brnardic, C.; Xu, S.; Asher, S. A. *J. Chem. Phys.* **1991**, *94*, 711−717.
(12) Kesavamoorthy, R.; Jagannathan, S.; Rundquist, P. A.; Asher, S. A. *J. Chem. Phys.* **1991**, *94*, 5172−5179.
(13) Rundquist, P. A.; Kesavamoorthy, R.; Jagannthan, S.; Asher S. A. *J. Chem. Phys.* **1991**, *95*, 8546−8551.
(14) Flaugh, P. L.; O'Donnell, S. E.; Asher, A. S. *Appl. Spectrosc.* **1984**, *38*, 847−850.
(15) Asher, S. A.; Flaugh, P. L.; Washinger, G. *Spectroscopy* **1986**, *1*, 26−31.
(16) Pan, G. S.; Kesavamoorthy, R.; Asher, S. A. *Phys. Rev. Lett.* **1997**, *78*, 3860−3863.
(17) Pan, G. S.; Kesavamoorthy, R.; Asher, S. A. *J. Am. Chem. Soc.* **1998**, *120*, 6525−6530.
(18) Holtz, J.; Weissman, J.; Pan, G.; Asher, S. A. *Mater. Res. Soc.* **1998**, *23*, 44−50.
(19) Yablonovitch, E. *J. Phys.: Condens. Matter* **1993**, *5*, 2443−2460.
(20) Joannopoulos, J. D.; Meade, R. D.; Winn, J. N. *Photonic Crystals*; Princeton University Press: Princeton, NJ, 1995.
(21) Ho, K. M.; Chan, C. T.; Soukoulis, C. M. *Phys. Rev. Lett.* **1990**, *65*, 3152−3155.
(22) Yablonovitch, E.; Gmitter, T. J. *Phys. Rev. Lett.* **1991**, *67*, 2295−2298.

10.1021/cm010811h CCC: $22.00
Published on Web 11/29/2001

electromagnetic radiation in particular spectral intervals and thus would show many unusual properties, with profound technological implications.[9,10,19,20]

Unfortunately, it appears that fcc or bcc CCA photonic crystals that contain dielectric spheres in lower refractive index media cannot show 3-D photonic band gaps.[19] Other crystal structures, such as the diamond structure,[21] for example, can show 3-D photonic band gaps. However, at present, methods to promote the self-assembly of these types of structures have not been demonstrated.

It has been suggested that optically anisotropic spherical colloidal particles[22−24] could be used to chemically fabricate 3-D photonic band gap materials. The anisotropy would perturb the fcc array symmetry[10] sufficiently enough to split the degeneracy of the Brillouin zone. This might increase the angular width of the photonic band gaps to approach the requirements for a 3-D photonic band gap material. Unfortunately, spherical colloidal particles cannot form anisotropic arrays unless the spherically symmetric interparticle interaction symmetry is perturbed.

Here, we demonstrate the fabrication of novel magnetically controllable photonic crystals formed through the self-assembly of highly charged, monodisperse superparamagnetic colloidal spheres. These superparamagnetic, monodisperse, and charged polystyrene particles, containing nanoscale iron oxide nanoparticles, were synthesized through emulsion polymerization.[25,26] They self-assemble into CCAs in deionized water and Bragg diffract visible light.

The diffraction from these superparamagnetic CCAs can be controlled by the imposition of magnetic fields, which readily alter the CCA lattice constant. We also observe magnetically induced self-assembly of these superparamagnetic particles into CCAs in media such as NaCl solutions and organic polar solvents, which normally do not permit spontaneous CCA self-assembly.

We find that magnetic fields can strain the fcc lattice of the superparamagnetic CCAs polymerized within hydrogels.[27−29] The lattice symmetry of this photonic crystal becomes tetragonal. Thus, this magnetically induced CCA self-assembly enables the development of novel photonic crystal materials and applications.

Experimental Section

Synthesis of Iron Oxide Nanoparticles. Nanoscale iron oxide was prepared by the coprecipitation of ferric and ferrous ions in ammonium hydroxide solution.[30−34] A 10.8 g portion of $FeCl_3 \cdot 6H_2O$ (J. T. Baker) and 4.0 g $FeCl_2 \cdot 4H_2O$ (Sigma) were dissolved in 50 mL of water. The resulting solution was poured with vigorous stirring into 500 mL of a 1.0 M NH_4OH solution. The resulting black precipitate was collected with a magnet. A 500 mL portion of 1 M tetramethylammonium hydroxide (TMAOH, Aldrich) solution was added to the precipitate, and the mixture was sonicated for 1 h. After that, 6.3 g of oleic acid and 1.0 g of sodium dodecyl benzene sulfonate (SDBS, Alcolac) were added to modify the magnetic colloid surface properties.[35]

Synthesis of Superparamagnetic Polymer Particles. We modified the procedure of Yanase[26] to produce superparamagnetic, highly charged, and monodisperse polystyrene−iron oxide composite colloidal particles. These particles were synthesized by emulsion polymerization of styrene by using a jacketed cylindrical reaction vessel that contained a reflux condenser, a Teflon mechanical stirrer, and a nitrogen/reagent inlet. The temperature was maintained through the jacket with the use of a circulating temperature bath. A nitrogen blanket and a stirring rate of 350 rpm were maintained throughout the polymerization.

The reaction vessel containing 180 mL of water and 20 mL of the above iron oxide dispersion was deoxygenated for 30 min. A 30 mL portion of styrene (St, Aldrich), 3.0 mL of methyl methacrylate (MMA, Aldrich), and 0.2 g of sodium styrene sulfonate (NaSS, Polyscience) were then added, and the temperature was increased to 70 °C when 2.0 g of APS (ammonium persulfate, Aldrich) was added to initiate the polymerization. The polymerization was carried out for 5 h.

The emulsion polymerization product appeared brown. A magnet was used to harvest the particles containing the iron oxide nanoparticles. We estimated from the magnetization measurements and the reaction stoichiometry that ∼3.5% of the polystyrene particles contained iron oxide particles.

Characterization of Nanosize Iron Oxide and Magnetic Polymer Composite Particles. X-ray powder diffraction studies utilized a Philips X'PERT system. A Zeiss EM 902A was used to measure the transmission electron micrographs. Energy dispersive X-ray fluorescence spectrometry (EDS, JEOL 35 CF) was used for qualitative elemental determinations. Flame atomic absorption was used to quantitatively measure the iron oxide content in the polystyrene−iron oxide composite particles. The surface charge density was determined by conductometric titrations of the particles with NaOH. A Brookhaven Z-90 plus light scattering photometer was used to measure hydrodynamic diameters and the ζ-potentials.

A Quantum Design MPMS superconducting quantum interference device (SQUID) magnetometer was used to determine the magnetic properties of the iron oxide nanoparticles and the polystyrene−iron oxide composite particles at room temperature between ±50 KOe.

Polymerized CCA Fabrication. The suspension of polystyrene−iron oxide composite particles, which was dialyzed against pure water and then further deionized with ion-exchange resin, self-assembles intoCCAs due to the electrostatic repulsion between these highly charged particles.

Polymerized CCAs (PCCAs)[27−29] were prepared by dissolving acrylamide (Fluka) or hydroxyethyl methacrylate (HEMA, Polysciences), cross-linkers such as *N*,*N*-methylenebisacrylamide (BAM, Fluka) or ethylene glycol dimethacrylate (EGDMA), and a UV photoinitiator such as diethoxyacetophenone (DEAP, Acros) in a diffracting suspension containing the polystyrene−iron oxide composite particles. This mixture was injected into a cell consisting of two quartz plates, separated by a 125 μm Parafilm spacer. The cell was exposed to UV light from a Blak-Ray (365 nm) mercury lamp to initiate polymerization. After 60 min of exposure, the PCCA was removed from

(23) Haus, J. W.; Sozuer, H. S.; Inguva, R. *J. Mod. Opt.* **1992**, *39*, 1991−2005.
(24) Li, Z. Y.; Wang, J.; Gu, B. Y. *Phys. Rev. B* **1998**, *58*, 3721−3729.
(25) Noguchi, H.; Yanase, N.; Uchida, Y.; Suzuta, T. *J. Appl. Polym. Sci.* **1993**, *48*, 1539−1547.
(26) Yanase, N.; Noguchi, H.; Asakura, H.; Suzuta, T. *J. Appl. Polym. Sci.* **1993**, *50*, 765−776.
(27) Asher, S. A.; Holtz, J.; Liu, L.; Wu, Z.; *J. Am. Chem. Soc.* **1994**, *116*, 4997−4998.
(28) Holtz, J. H.; Asher, S. A. *Nature* **1997**, *389*, 829−832.
(29) Weissman, J. M.; Sunkara, H. B.; Tse, A. S.; Asher, S. A. *Science* **1996**, *274*, 959−960.
(30) Kang, Y. S.; Risbud, S.; Rabolt, J. F.; Stroeve, P. *Chem. Mater.* **1996**, *8*, 2209−2211.
(31) Sauzedde, F.; Elaissari, A.; Pichot, C. *Colloid Polym. Sci.* **1999**, *277*, 846−855.
(32) Liz, L.; Quintela, A.; Mira, J.; Rivas, J. *J. Mater. Sci.* **1994**, *29*, 3797−3801.
(33) Perez, J. A.; Quintela, M. A.; Mira, J.; Rivas, J.; Charles, S. W. *J. Phys. Chem. B* **1997**, *101*, 8045−8047.
(34) Lee, J.; Isobe, T.; Senna, N. *J. Colloid Interface Sci.* **1996**, *177*, 490−494.
(35) Shimoiizaka, J.; Nakatsuka, K.; Chubachi, R.; Sato, Y. *Nippon Kagaku Kaishi* **1976**, 6−9.

Table 1. Comparison of X-ray Diffraction Measurements of Our Iron Oxide Nanoparticles and Polystyrene−Iron Oxide Nanocomposite Particles to That of Different Iron Oxide Structures

nanoscale iron oxide		PSt composite	bulk γ-Fe_2O_3		bulk Fe_3O_4	
d (Å)	intensity	*d* (Å)	*d* (Å)	intensity	*d* (Å)	intensity
2.95	37	2.94	2.95	34	2.97	70
2.51	100	2.52	2.52	100	2.53	100
2.10	30	2.09	2.08	24	2.10	70
1.70	18	1.70	1.70	12	1.71	60
1.61	40	1.61	1.61	33	1.61	85
1.48	56	1.48	1.48	53	1.48	85

the cell. Alternatively, the PCCA was thermally polymerized using 2,2′-azobisisobutyronitrile (AIBN, Aldrich) as the initiator. The polymerization was performed at 65 °C for 2 h.

Diffraction Measurements. The diffraction spectra of the CCA and PCCA were measured by using a model 440 CCD UV−vis spectrophotometer (Spectral Instruments, Inc.) coupled to a 6 around 1 reflectance probe optical fiber. Transmission measurements were measured by using a Perkin-Elmer Lambda 9 absorption spectrophotometer. The CCA and PCCA samples were oriented normal to the incident light beam.

Results and Discussion

1.0. Characterization of Superparamagnetic Polystyrene Particles. *1.1. X-ray Diffraction Characterization.* We used X-ray diffraction (XRD) to determine the structure of our iron oxide nanoparticles, which were produced by coprecipitation of ferric and ferrous chloride in ammonia, and of our polystyrene−iron oxide composite particles (Figure 1). The XRD spectra are identical, indicating that the iron oxide structure was not changed during the emulsion polymerization.

There are many different possible iron oxide structures such as magnetite (Fe_3O_4), hematite (α-Fe_2O_3), maghemite (γ-Fe_2O_3), or ferric hydroxide (β-FeOOH). Although our particles show XRD *d* spacings close to those of both magnetite and maghemite, which are inverse spinel structures, the relative diffraction intensities indicate that they are closer to maghemite than magnetite (Table 1). The increased oxygen content may result from the oxidation of our particles in air.[31−34]

1.2. Transmission Electron Microscopy Measurements. Figure 2 shows transmission electron microscopy (TEM) of the iron oxide nanoparticles and the polystyrene−iron oxide composite particles. The iron oxide nanoparticles have a broad size distribution (2−15 nm) with an average diameter of ∼10 nm.

The polystyrene−iron oxide composite particles have a number average particle diameter of 134 nm (essentially identical to their hydrodynamic diameter measured by light scattering in 5 mM KCl). These particles show a polydispersity of 7.5%. TEM shows that the iron oxide particles occur as clumps within the polystyrene particles. EDS (Figure 3) shows the expected iron peaks.

1.3. Magnetization Measurements. Figure 4 shows SQUID magnetometer measurements of the iron oxide nanoparticles and the polystyrene−iron oxide composite particles. Neither coercivity nor remanence was observed. Thus, the particle magnetic moments relax to their equilibrium magnetic state within the measurement time. Thus, these monodisperse polystyrene−iron oxide composite particles are superparamagnetic and, as shown below, are attracted to regions of high magnetic field divergence, ∇H. The saturation magnetizations of the iron oxide nanoparticles and polystyrene−iron oxide composite particles are 72.8 and 12.7 emu g^{-1}, respectively. This ratio of saturation magnetization (17.4%) is essentially identical to the weight fraction of iron oxide in the polystyrene−iron oxide composite particles found by atomic absorption measurements (17.0 wt %, assuming Fe_2O_3). The average saturation magnetic moment per polystyrene−iron oxide composite particle, μ_{pt}, is 1.48×10^{-14} emu.

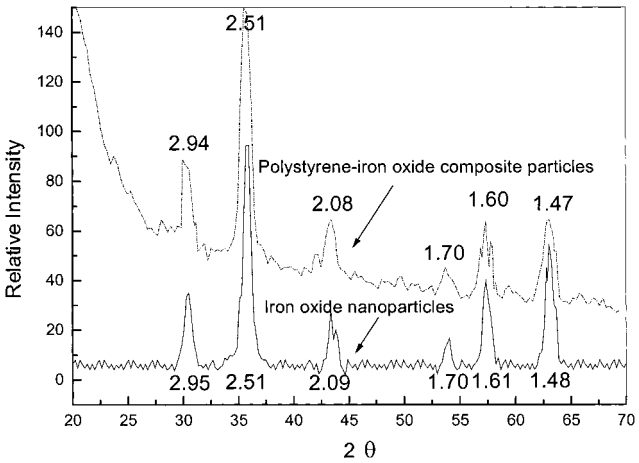

Figure 1. X-ray powder diffraction pattern (Cu Kα radiation) of the nanoscale iron oxide and polystyrene−iron oxide composite particles. The lattice spacings (in Å) and the relative diffraction intensities indicate that the iron oxide structure is γ-Fe_2O_3.

1.4. Colloidal Particle Surface Charge. Our conductometric titration measurements show a polystyrene−iron oxide composite particle surface charge density of 6.3 μC cm^{-2}. We measure a ζ-potential of −55 mV for these particles in a 5 mM KCl solution.

2.0. Magnetic Field Induced Superparamagnetic CCA Self-Assembly. *2.1. Effect of Magnetic Field on the Self-Assembly in Deionized Water.* These superparamagnetic, monodisperse, and highly charged particles self-assemble in deionized water into CCAs that Bragg diffract light in the visible region. In the absence of a magnetic field, their spontaneously self-assembled CCA lattice constant is determined solely by the particle number density and the crystal structure.

When a permanent magnet is brought close to the CCA, an additional force $F_m = \nabla(\mu H)$ occurs, which causes the superparamagnetic particles to be attracted to the local magnetic field gradient maximum, where μ is the magnetic field dependent particle magnetic moment. Based on the magnetization curve shown in Figure 4, we calculated a magnetic packing force, $F_m = -4.0 \times 10^{-11}$ dynes per particle, for a 2.7 KOe magnetic field with a gradient of 3.56 KOe cm^{-1}.

The presence of the magnetic field induces a magnetic moment, which generates an interparticle magnetic moment−magnetic moment repulsive force, $F_{mr} = 3(\mu_{Pt}^2/d^4)$, in the plane perpendicular to the magnetic field and an attractive interparticle force in the direction parallel to the field, $F_{ma} = -6(\mu_{Pt}^2/d^4)$. In the presence of a 2.7 KOe magnetic field with a gradient of 3.56 KOe cm^{-1}, the nearest-neighbor spacing of our particles is (center-to-center) $d = 198.6$ nm (Figure 6).

Using the above interparticle magnetic moment interaction expressions, we calculated a maximum mag-

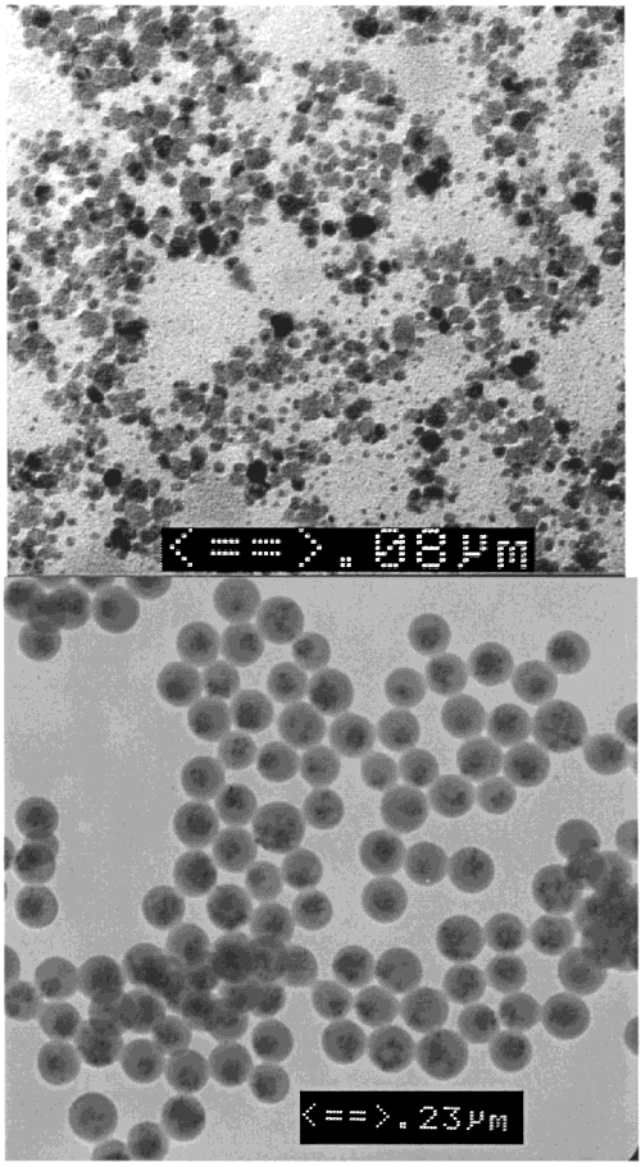

Figure 2. Transmission electron microscopy measurement of nanoscale iron oxide (top) and polystyrene−iron oxide composite particles (bottom). The iron oxide particles have a broad size distribution from 2 to 15 nm, with a number average diameter of ∼10 nm. The polystyrene particle average diameter is 134 nm, with a polydispersity of 7.5%. The aggregates of iron oxide nanoparticles appear as black dots in the center of the larger polystyrene−iron oxide composite particles.

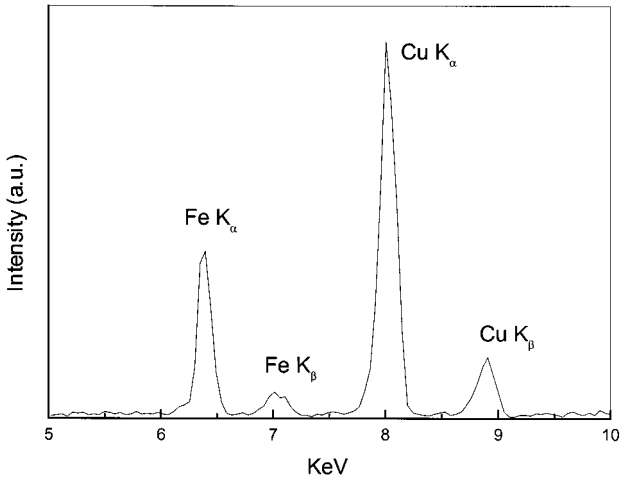

Figure 3. Energy dispersive X-ray fluorescence spectrometry of polystyrene−iron oxide composite particles. The peak due to Fe is clearly evident, while the strong Cu peak is derived from the copper grid used to support the sample.

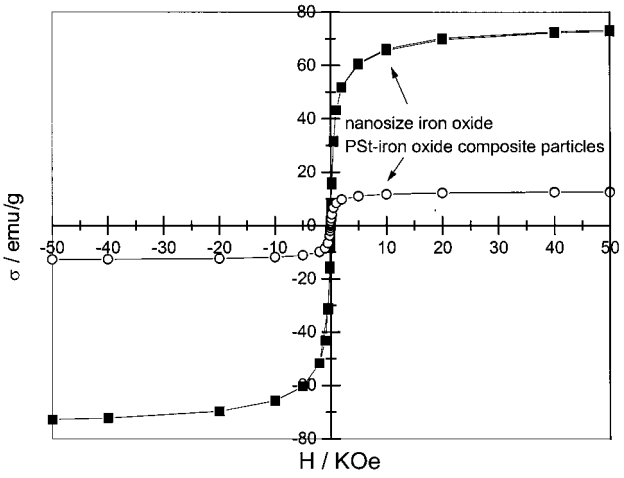

Figure 4. SQUID measurements of nanoscale iron oxide and polystyrene−iron oxide composite particles at room temperature. Neither coercivity nor remanence was observed for both samples. The lack of hysteresis indicates that these particles are superparamagnetic.

netic dipole repulsive force in the plane perpendicular to the external magnetic field of $F_{mr} = 4.2 \times 10^{-9}$ dynes per particle and a maximum interparticle magnetic dipole attractive force parallel to the external magnetic field of $F_{ma} = -8.4 \times 10^{-9}$ dynes per particle. These forces are ∼50-fold smaller than the interparticle electrostatic repulsive force, $F_{er} = \pi\epsilon\zeta^2\kappa a e^{-\kappa h} = 4.0 \times 10^{-7}$ dynes per particles (a dielectric constant $\epsilon = 78.4$, a ζ-potential $\zeta = -55$ mV, a Debye length $1/\kappa = 15$ nm, a particle radius $a = 67$ nm, and an interparticle surface-to-surface distance $h = 68$ nm).

The presence of a 2.7 KOe magnetic field with a gradient of 3.56 KOe cm^{-1} causes a 5.2 nm mm^{-1} gradation of the nearest-neighbor particle distance along the field. We can model this phenomenon, most simply, if we consider a square lattice of spherical particles and consider layers 1, 2, and 3 in detail (Figure 5). Given that the Figure 5 magnetic field diverges toward the right, the nearest particle distance d_{12} is slightly smaller than d_{23}. The uniaxial magnetic field packing force, $F_m = -4.0 \times 10^{-11}$ dynes per particle, compresses the lattice and establishes a static equilibrium balance between the magnetic packing force and the electrostatic repulsive force between particles.

We calculate that the magnetic dipole−magnetic dipole attractive forces between particles along the field direction is much smaller than the difference in the electrostatic repulsive forces between particles. For example, for particle 2, $F_{ma,12} - F_{ma,32} = 1.5 \times 10^{-13}$ dynes per particle, while $F_{er,12} - F_{er,32} = 2.9 \times 10^{-11}$ dynes per particle. The lattice constant is essentially determined by the balance between the magnetic packing force and the interparticle electrostatic repulsive force. The lattice constant should be a minimum at the locus of the magnetic field gradient maximum and should increase as the gradient decreases.

The magnetic dipole−magnetic dipole interaction terms should lead to a tetragonal distortion of the fcc

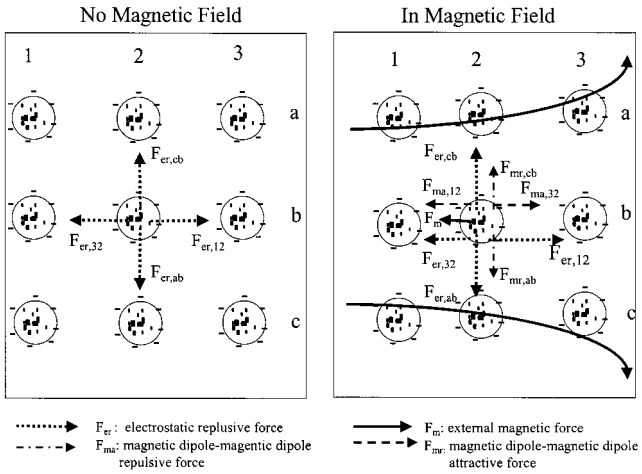

Figure 5. Forces on superparamagnetic particles within a CCA in the absence and presence of a magnetic field. In the absence of a magnetic field, the interparticle electrostatic repulsive forces F_{er} balance each other. The magnetic field induces additional magnetic packing forces, F_m, additional magnetic dipole−magnetic dipole repulsive forces, F_{mr} that are perpendicular to the magnetic field, and additional magnetic dipole attractive forces, F_{ma} that are parallel to the magnetic field. The CCA is compressed along the magnetic field. Thus, the magnetic packing force F_m on layer 2 is balanced by both the electrostatic repulsive force ($F_{er,12}-F_{er,32}$) and the magnetic dipole−magnetic dipole attractive force ($F_{ma,12}-F_{ma,32}$).

lattice, where the interparticle spacing increases in the plane perpendicular to the field, while along the field the interparticle spacing decreases. We can roughly estimate the magnitude of this change by calculating the DLVO interparticle distance change required to balance the additional forces. We estimate that the resulting tetragonal distortion would be associated with ∼0.1% of alterations in the interparticle distances. This small tetragonal distortion will be difficult to measure experimentally. Therefore, we see no difference between the diffraction normal and parallel to the external magnet field.

Figure 6 shows the observed influence of a magnetic field on a thick CCA assembly of superparamagnetic particles. The diffraction peaks, shown in the Figure 6 insert, result from the CCA 111 fcc planes, which are the most densely packed and are oriented parallel to the glass surface. For 180° backscattering, the diffraction peak blue-shifts from ∼560 to ∼428 nm as the magnetic field gradient increases from 1.5−5.4 KOe cm^{-1}. Using Bragg's law for the CCA ($\lambda_o = 2nd \sin\theta$, where λ_o is the wavelength of the diffracted light in a vacuum, n is the average CCA refractive index, d is the 111 plane spacing, and $\theta = 90°$ is the Bragg glancing angle), we calculate[3] that the 111 plane spacing decreases from 206 to 153 nm. As expected, the plane spacing is a minimum at the locus of the magnetic field gradient maximum and increases as the gradient decreases.

We also measured the magnetic field dependence of diffraction from a thin superparamagnetic CCA (Figure 7). In the absence of a magnetic field, this sample diffracts 910 nm light. The 910 nm peak results from diffraction by the fcc 111 plane, while the peak at half this wavelength (455 nm) results from second-order diffraction from a host of planes that fortuitously diffract simultaneously.[36] Usually, the second-order diffraction is much more intense than the first-order diffraction.[36] Presumably, the decreased second-order intensity results from absorption by the iron oxide nanoparticles.

As this thin sample is translated toward the magnet, the diffraction wavelength observed in back diffraction decreases from 904 to 850 nm, where the field divergence maximizes at 4.7 KOe cm^{-1}. As expected, the lattice spacing varies linearly with the magnetic field gradient, since the magnetic packing force is proportional to the gradient of the magnetic field.

This experiment also demonstrates that the diffraction of this spontaneously self-assembled CCA can be controlled by magnetic fields. To our knowledge, this is the first example of a magnetically controlled photonic crystal.

2.2. Magnetic Field Induced CCA Self-Assembly. Normally, CCA self-assembly does not occur spontaneously in high ionic strength aqueous solutions or in organic solvents, due to the screening of the electrostatic repulsion between colloidal particles. However, these superparamagnetic particles can be magnetically induced to self-assemble into CCAs within high ionic strength aqueous solutions and in polar organic solvents.

When an external magnetic field is applied to the dispersion of superparamagnetic particles, the field gradient exerts a force on the particles and induces a slow phase separation of the superparamagnetic particles into a high volume fraction phase near the wall of the sample holder. These particles slowly pack into highly ordered CCAs at the container wall. Although a similar high volume fraction (∼20%) of these charged colloidal particles would show some ordering, highly ordered CCAs would not be formed since the high particle volume fraction would be too viscous to allow the CCAs to anneal into a well-ordered fcc structure. The system would form a glassy state.

This magnetic self-assembly mechanism is probably similar to the mechanisms responsible for the formation of close-packed CCA ordering during gravitational settling and the mechanism responsible for the formation of close-packed CCA ordering during fluid flow assembly,[39] under oscillatory shear,[40] or evaporative deposition,[41] where the 111 fcc crystal planes grow out from the surface as the next layer of particles pack against the previously stacked layer.

Figure 8A shows diffraction spectra of magnetically assembled CCAs in solutions of increasing NaCl concentrations. In pure water, the 111 plane of the fcc lattice diffracts ∼620 nm light, while in 0.16 mM NaCl, the diffraction blue-shifts to 575 nm and further blue-shifts to 420 nm for a 4 mM NaCl concentration. Thus, these superparamagnetic particles pack more densely as the screening increases for the higher NaCl ionic strengths. It is somewhat surprising that we observe a minimum neighbor spacing as large as ∼180 nm, since

(36) Liu, L.; Asher, S. A. *J. Am. Chem. Soc.* **1997**, *119*, 2729−2732.
(37) Sogami, I.; Ise, N. *J. Chem. Phys.* **1984**, *81*, 6320−32.
(38) Tomita, M.; Ven, T. G. M. *J. Phys. Chem.* **1985**, *89*, 1291−1296.
(39) Parik, S. H.; Xia, Y. *Langmuir* **1999**, *15*, 266−273.
(40) Vickreva, O.; Kalinina, O.; Kumacheva, E. *Adv. Mater.* **2000**, *12*, 110−102.
(41) Jiang, P.; Bertone, J. F.; Hwang, K. S.; Colvin, V. L. *Chem. Mater.* **1999**, *11*, 2132−2140.

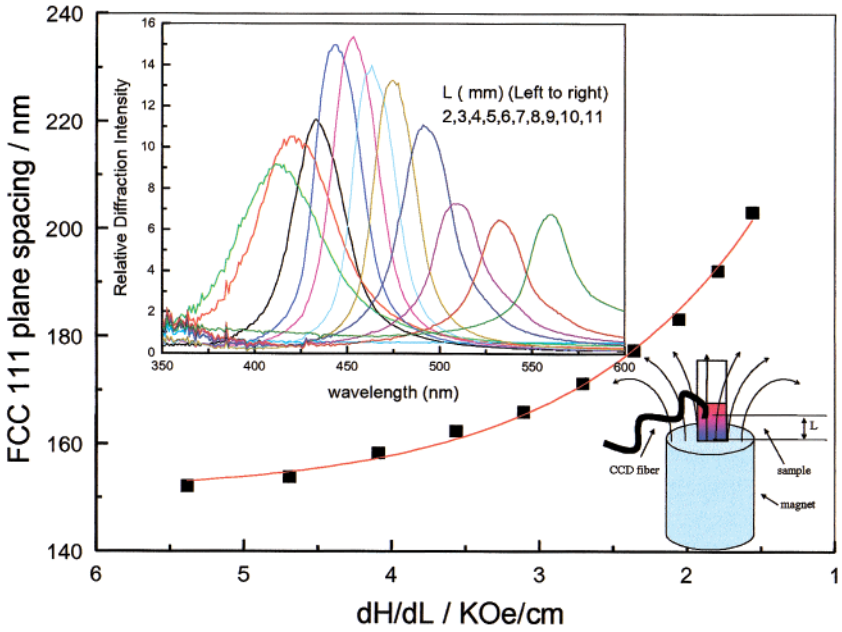

Figure 6. Influence of the average magnetic field gradient, d*H*/d*L*, on the lattice constant of a thick CCA composed of 134 nm superparamagnetic particles in deionized water (4.2 vol %). The top inset shows the dependence of the diffraction peak wavelength on the distance from the magnet. In the lower right is an experimental schematic showing the CCA on top of a permanent magnet. A reflectance optical fiber probe connected to a CCD spectrometer is used to measure the diffraction spectrum. The spatial dependence of the magnetic field strength was measured by using a Hall probe.

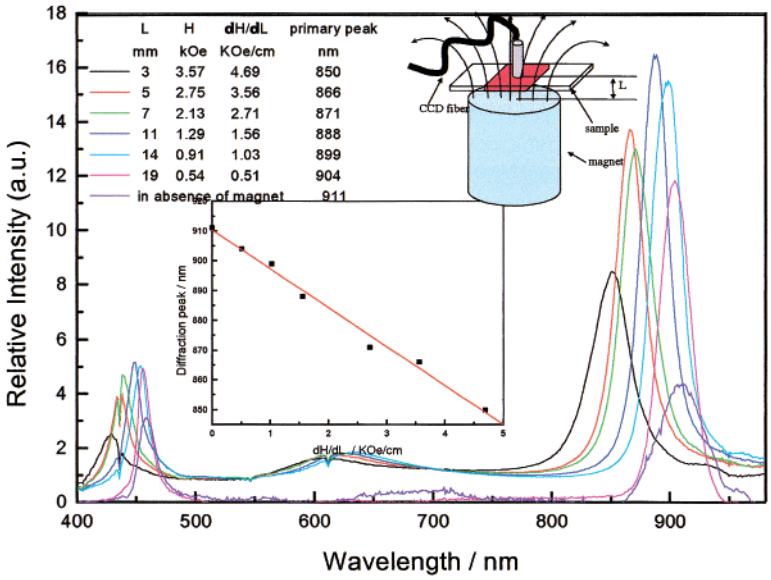

Figure 7. Influence of a magnetic field on the packing of a thin CCA composed of 134 nm superparamagnetic particles in deionized water (2.5 vol %). The inset shows the linear dependence of the diffraction wavelength on the magnetic field gradient. The diffracted wavelength linearly decreases from 904 to 850 nm as the sample is translated to increase the magnetic gradient.

the actual particle diameter is 134 nm and because 4 mM NaCl solutions have short Debye lengths of 4.8 nm.[37]

Figure 8B shows diffraction spectra of superparamagnetic magnetically self-assembled CCAs in a series of organic solvents. In pure water, the 111 plane diffracts ~530 nm light. The diffraction blue-shifts to 495 nm in dimethyl sulfoxide and to 450 nm in acetonitrile and further blue-shifts to 400 nm in ethanol. The 111 plane spacing decreases linearly as the solvent dielectric constant decreases, as expected from the DLVO theory, which predicts that the electrostatic repulsive forces are proportional to the dielectric constant.[37,38]

3.0. Fabrication of Solid Photonic Crystals. The CCA fluid photonic crystals were rigidized into soft solids by embedding the CCAs into hydrogel polymer matrixes. Previous hydrogel polymerizations to form PCCA required the use of photochemical polymerization to avoid ionic species that would screen the interparticle repulsive interactions which would decrease the CCA ordering.[27−29] In contrast, the magnetically assembled superparamagnetic CCAs can be polymerized in a variety of solvents and by using a variety of initiators.

For example, we assembled our CCA in a deionized aqueous solution, which contained 0.0993 gm mL^{-1} of AM, 0.003 gm mL^{-1} of BAM, and 0.005 gm mL^{-1} of

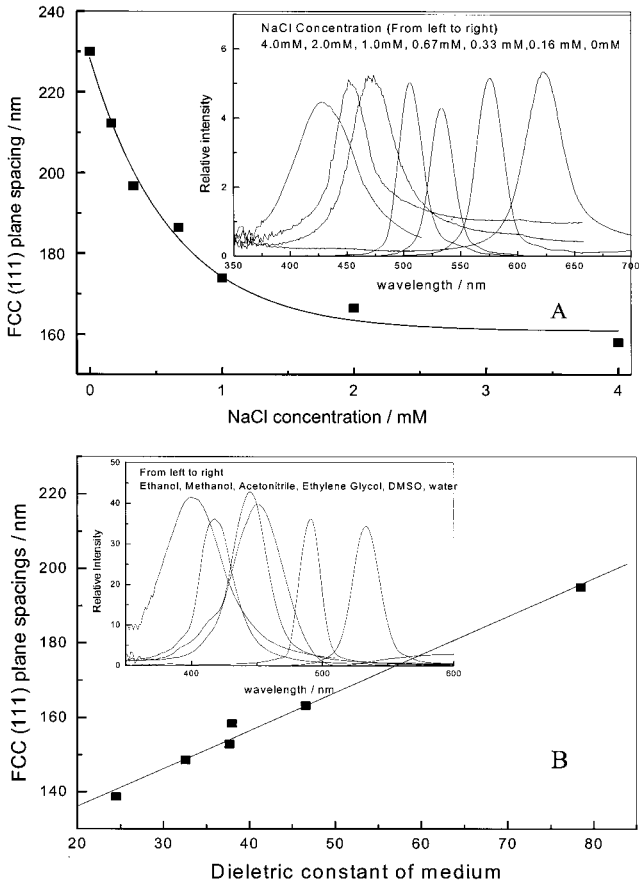

Figure 8. Magnetic field induced packing of superparamagnetic particles in different media in a 4.6 KOe magnetic field with a 6.2 KOe cm^{-1} gradient: (A) magnetic assembly from a 5% particle volume fraction NaCl aqueous solution; (B) magnetic self-assembly from 10% particle volume fraction dispersions in ethanol (24.5), methanol (32.6), acetonitrile (37.7), ethylene glycol (38), DMSO (46.6), and water (78). The dielectric constant of each solvent is given in parentheses.

AIBN (the thermal initiator). In the absence of a magnetic field, we introduced this CCA solution into a thin cell which we heated to 60 °C to polymerize the PCCA. Figure 9 shows that this magnetically assembled CCA diffracted 450 nm light before and after polymerization. This PCCA had only ~3% cross-linking. After polymerization, we removed this PCCA from the cell and exposed it to deionized water, which caused the hydrogel to swell and the lattice to expand, which red-shifted the diffraction to 580 nm.

These PCCA hydrogels can also be polymerized in the presence of magnetic fields under conditions that are incompatible with spontaneous CCA self-assembly. Figure 10 shows the reflection spectra of PCCAs fabricated by the thermal polymerization of AM and BAM in water and by the thermal polymerization of HEMA and EGDMA in ethanol.

As discussed above, the magnetic field can induce a gradient in the lattice constant, where the diffraction wavelength decreases with increased distance from the magnet (Figure 6). This permits fabrication of PCCA photonic crystals where the diffraction wavelengths vary as a function of position.

4.0. Magnetic Response of PCCA. Superparamagnetic PCCA are soft elastic materials that should respond to magnetic fields. Figure 11 shows the mag-

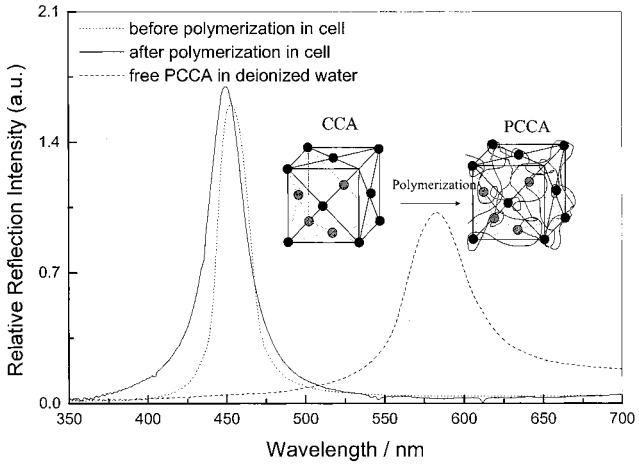

Figure 9. Reflection spectra of CCA in deionized water before and after a thermal hydrogel polymerization initiated with AIBN. The low cross-linking of the PCCA volume resulted in a significant swelling and diffraction red-shift upon removing the PCCA from the polymerization cell and exposing it to deionized water.

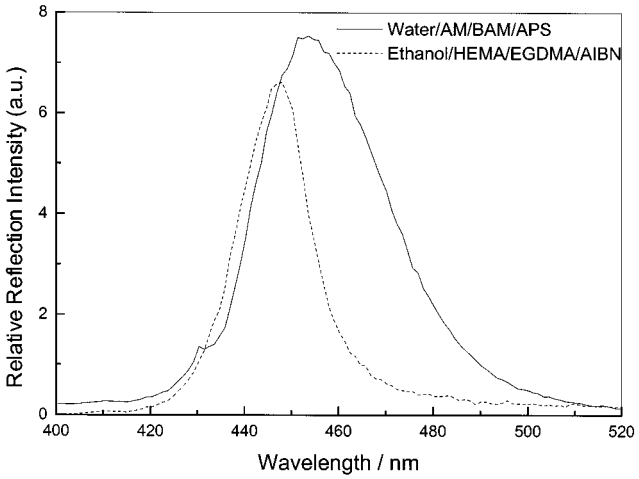

Figure 10. Reflection spectra of PCCA formed by the magnetic assembly of a CCA polymerized in situ, in media which are incompatible with spontaneous CCA self-assembly: (A) aqueous solution containing 7.7 mM APS; (B) ethanol.

netic response of a 500 μm thick PCCA film of superparamagnetic particles made by the thermal polymerization of AM and BAM. One end of the film was held stationary. A magnet was placed next to the free end. The diffraction was measured normal to the film plane. The diffraction from this superparamagnetic PCCA promptly blue-shifted from 787 to 783 nm and, over a period of 60 min, slowly blue-shifted to its equilibrium diffraction of ~777 nm. The magnetic field induced diffraction shift was fully reversible (Figure 11); removal of the magnet caused the diffraction to shift back to its original 787 nm diffraction.

The magnetically induced diffraction shift presumably results from a uniaxial strain on the PCCA. The anisotropic strain induced by the magnetic field elongates the lattice constant along the field direction. Conservation of volume decreases the lattice constant along directions normal to the strain direction and thus decreases the 111 plane lattice constant and blue-shifts the diffraction wavelength. Thus, magnetic fields can be used to tune the diffraction wavelength. Although the diffraction wavelength shift is relatively small in

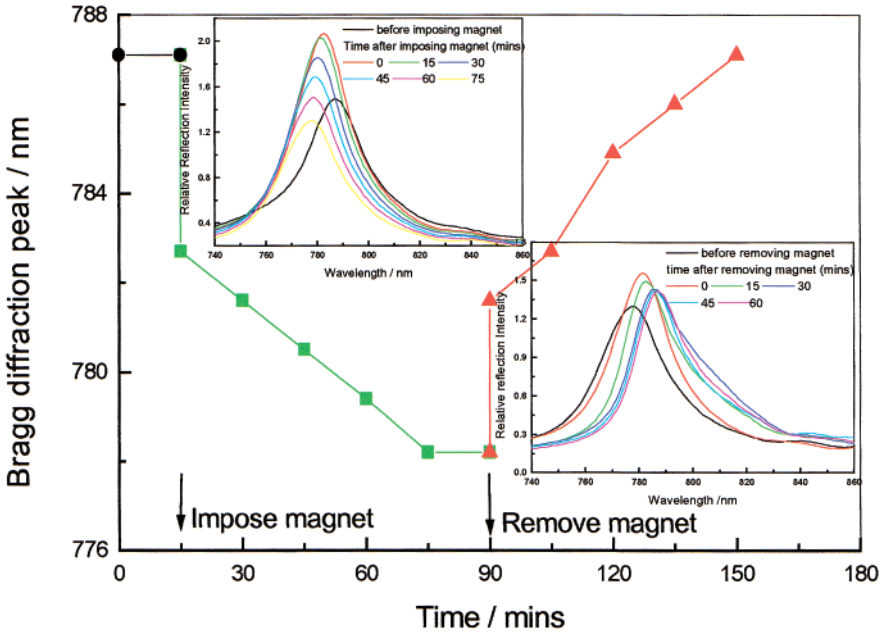

Figure 11. Response of superparamagnetic PCCA film to a 2.4 KOe magnetic field with a 3.2 KOe cm^{-1} gradient. After imposition of the magnetic field, the Bragg diffraction blue-shifted from 787 to 777 nm. This shift was fully reversible; the diffraction red-shifted back to 787 nm after removing the magnetic field.

this example, the use of higher magnetic fields or the use of more elastic superparamagnetic PCCA would give larger wavelength tuning.

The unixial strain on the PCCA causes an anisotropy in the fcc lattice constant, where the lattice constant along the field lines increases while the lattice constants that are perpendicular decrease. Thus, the crystal symmetry changes from the cubic symmetry of the fcc lattice to tetragonal symmetry. This may have significant consequences for the PCCA diffraction properties. These tetragonal lattices may prove to be useful in the fabrication of 3-D photonic band gap materials.

Conclusions

We have demonstrated the fabrication of novel magnetically controllable photonic crystals formed through the self-assembly of highly charged, monodisperse superparamagnetic colloidal spheres. These superparamagnetic monodisperse charged polystyrene particles containing nanoscale iron oxide nanoparticles were synthesized through emulsion polymerization. They self-assemble into CCAs in deionized water and Bragg diffract visible light. The diffraction from these superparamagnetic CCAs can be controlled by applying magnetic fields, which readily alter the CCA lattice constant. We also observe magnetically induced self-assembly of these superparamagnetic particles into CCAs in media, such as NaCl aqueous solutions and organic polar solvent, which normally do not permit spontaneous CCA self-assembly. We also find that magnetic fields can strain the fcc lattice of superparamagnetic CCAs polymerized within hydrogels. The lattice symmetry of this photonic crystal becomes tetragonal. The observed magnetically induced CCA self-assembly enables the development of novel photonic crystal materials and devices.

Acknowledgment. We gratefully acknowledge Dr. Wei Wang for advice on the superparamagnetic colloid synthesis. We also thank Prof. Irving Lowe for helpful discussions about magnetism. S.A.A. also acknowledges support for this work from ONR Grant No. N00014-94-1-0592 and Darpa Contract No. DAAD16-99-R-1006. S.A.M. acknowledges support from NSF Grant No. CTS-9800128 and PRF Grant No. 33866-AC5.

CM010811H